Computational and Structural Biotechnology Journal 19 (2021) 5246–5254

COMPUTATIONAL AND STRUCTURAL BIOTECHNOLOGY JOURNAL

journal homepage: www.elsevier.com/locate/csbj

A structural view onto disease-linked mutations in the human neutral amino acid exchanger ASCT1

Pavlo Stehantsev [a,1], Artem Stetsenko [a,1], Mariia Nemchinova [a], Nanda Gowtham Aduri [b], Siewert J. Marrink [a], Cornelius Gati [b], Albert Guskov [a,c,*]

[a] Groningen Biomolecular Sciences and Biotechnology Institute, University of Groningen, The Netherlands
[b] Department of Biological Sciences, Bridge Institute, USC Michelson Center for Convergent Bioscience, University of Southern California, Los Angeles, CA, USA
[c] Moscow Institute of Physics and Technology, Dolgoprudny, Russia

ARTICLE INFO

Article history:
Received 30 July 2021
Received in revised form 14 September 2021
Accepted 14 September 2021
Available online 17 September 2021

Keywords:
Membrane transporter
Solute carrier
Cryo-EM
Molecular dynamics
ASCT1
Structural biology

ABSTRACT

The ASCT1 transporter of the SLC1 family is largely involved in equilibration of neutral amino acids' pools across the plasma membrane and plays a prominent role in the transport of both L- and D-isomers of serine, essential for the normal functioning of the central nervous system in mammals. A number of mutations in ASCT1 (E256K, G381R, R457W) have been linked to severe neurodevelopmental disorders, however in the absence of ASCT1 structure it is hard to understand their impact on substrate transport. To ameliorate that we have determined a cryo-EM structure of human ASCT1 at 4.2 Å resolution and performed functional transport assays and molecular dynamics simulations, which revealed that given mutations lead to the diminished transport capability of ASCT1 caused by instability of transporter and impeded transport cycle.

1. Introduction

Alanine Serine Cysteine Transporter 1 (ASCT1) belongs to the solute carrier 1 family (SLC1) of proteins, which includes the subfamily of Excitatory Amino Acid Transporters (EAAT1-5) and another neutral amino acid exchanger, ASCT2 [1–3]. EAATs use the sodium gradient as an energy source to re-uptake the neurotransmitter glutamate (as well as L- or D-aspartate) in the synaptic cleft to prevent the overstimulation of glutamate receptors and avoid excitotoxicity [4–6]. The transport is also coupled to H^+ and counter-transport of K^+ ion [7–9], and additionally all transporters reveal different levels of uncoupled chloride conductance [10–13].

ASCT proteins, in contrast, do not concentrate their substrates, but perform the obligatory exchange of the amino acid pools, although the transport is still coupled to Na^+ [14–16]. There is still no consensus whether the transport is electroneutral (this work and [14,15]) or electrogenic (discussed in [17]). ASCTs are ubiquitously expressed with the highest expression of ASCT2 in placenta, lung, skeletal muscle, kidney, pancreas, and intestine and of ASCT1 in brain, muscle, and pancreas [18–21]. ASCT2 has gained a lot of focus since it has been linked to numerous cancers (see recent reviews [22,23]) where it is involved into the transport of glutamine, which is essential for carcinogenesis as it can be used to fuel the TCA cycle [24]. Up to date ASCT1 was associated only with esophageal adenocarcinomas [25] and prostate cancer [26], albeit it was shown that ASCT1 is not capable to transport glutamine [27].

L-Ser is a non-essential amino acid, however there is an active de novo synthesis of L-Ser in the brain [28] as it is a critical precursor for the synthesis of L-Cys, phosphatidyl-L-Ser, sphingolipids, and most importantly of D-Ser [29,30]. D-Ser is a major co-agonist of N-methyl-D-aspartate receptors [31,32] produced by racemization of L-Ser by the specific enzyme serine racemase [33], which is heavily expressed in neurons, and to some extent in glial cells [34–36]. However the synthesis of L-Ser is confined to astrocytes [37], hence it must be somehow shuttled to serine racemase (so-called serine shuttle [38]), and the major role in L-Ser transport is ascribed to ASCT1 [39], which is capable to exchange L-Ser for D-Ser or any other suitable substrate. Interestingly, both ASCT1 and ASCT2 were shown to transport L-Ser and D-Ser in transfected HEK293 cells [40,41], hence perhaps there is an

* Corresponding author at: Groningen Biomolecular Sciences and Biotechnology Institute, University of Groningen, The Netherlands.
E-mail address: a.guskov@rug.nl (A. Guskov).
[1] These authors contributed equally to this work.

https://doi.org/10.1016/j.csbj.2021.09.015

interplay between two transporters with the preferential expression of ASCT1 in astrocytes [18,39] and ASCT2 in neurons [42].

Experiments on ASCT1-knock out mice revealed numerous motor and neurodevelopmental disorders [39] similar to those linked to nonsense and missense mutations in ASCT1 in humans (recently reviewed in [43]), which cause autosomal recessive neurodevelopmental disorders, generally termed as spastic tetraplegia, thin corpus callosum, and progressive microcephaly (SPATCCM, Online Mendelian Inheritance in Man # 616657). Up to date characterized nonsense mutations are Y191* (so only a partial scaffold domain and almost none of a transport domain produced), which leads to microcephaly, tonic-clonic seizures, motor and speech delays [44]; W453* (almost complete protein produced, except TM8 and C-terminus), leading to microcephaly, motor and dyscognitive seizures, speech delay [45]; one frame shift mutation L315*fs (hence the transport domain does not follow the canonical sequence), causing microcephaly, infantile spasms, speech delay [46]; and three missense mutations – E256K, G381R, R457W, leading to various degrees of similar disorders and disabilities [46–49].

To be able to map these mutations and get a better understanding how they lead to the malfunctioning of this transporter, we solved the ASCT1 structure using single-particle cryo-EM technique to the overall resolution of 4.2 Å and performed subsequent all-atom molecular dynamics (MD) simulations on the aforementioned missense mutations as well as their functional characterization.

2. Materials and methods

2.1. Transformation and cloning

The pPICZ-B vector with incorporated human wild-type ASCT1 gene was ordered from GenScript. Mutants E256K (forward primer 5′ CAATTCCCTCAACAAGGCGACGATGGTGCTGG 3′; reverse primer 5′ CCAGCACCATCGTCGCCTTGTTGAGGGAATTG 3′) and R457W (forward primer 5′ TGGATTGTGGACTGGACCACCACGGTGGTGAA 3′, reverse primer 5′ TTCACCACCGTGGTGGTCCAGTCCACAATCCA 3′) were introduced using QuickChange site-directed mutagenesis on the ordered pPICZ-B vector with the inserted human wild-type ASCT1 gene. The constructs were transformed into chemically competent *Escherichia coli* DH5α cells to produce ~ 10 μg of the plasmid. The isolated plasmids were linearised with *PmeI*, transformed into sorbitol-treated *P. pastoris* strain X-33 by electroporation, and grown on the Yeast Extract Peptone Dextrose (YPDS) medium agar plates at 30 °C for four days. Zeocin (Invitrogen) with 100 μg/mL, 500 μg/mL and 1000 μg/mL concentrations was used as a selection marker. For analysis, a few colonies from each plate were picked and grown in 5 mL Yeast Extract Peptone Dextrose (YPD) medium with 100 μg/mL Zeocin (Invitrogen) in CELLSTAR® CELLreactor tubes at 30 °C, 200 rpm, overnight.

2.2. Protein expression and purification

For large-scale protein production, the transformed cells were pre-cultured in 1 l baffled flask with 100 mL of the Buffered Glycerol-complex (BMGY) medium without antibiotics at 30 °C, 200 rpm, overnight. The next day, the medium was replaced with the Buffered Methanol-complex (BMMY) setting up the start OD_{600} to 1.0 in 500 mL. The cells were expressed for 72 h in a 5 l baffled flask at 30 °C, 200 rpm, with addition of 0.5% methanol for every 24 h period.

Further, the cells were isolated by centrifugation (4,500 g, 10 min, 4 °C), resuspended in Buffer A (50 mM Tris-HCl, pH 7.4, 250 mM NaCl, 5% (vol/vol) glycerol), flash frozen in liquid nitrogen and stored at −80 °C. The cells were broken with Maximator High Pressure Homogenizer Type HPL6 (Maximator GmbH). The cells were supplied with 0.1 mg ml^{-1} DNase (Sigma-Aldrich) and 3 mM $MgSO_4$, and broken in three passages (39 kPsi, 4 °C). After the second passage, the broken cells were supplied with 1 mM phenylmethylsulfonyl fluoride (Roche) protease inhibitor. The cell lysate was centrifuged (10,000 g, 30 min, 4 °C) to remove cell debris, and the supernatant was ultracentrifuged (194,000 g, 120 min, 4 °C) to sediment membrane fractions. The membrane fractions were resuspended in Buffer B (50 mM Tris-HCl, pH 7.4, 250 mM NaCl, 5% (vol/vol) glycerol), flash frozen and stored at −80 °C in aliquots of membrane vesicles from ~ 2.5 g cells.

To purify the wild-type or mutant proteins, an aliquot of the membrane vesicles was kept with Buffer C (50 mM Tris-HCl, pH 7.4, 250 mM NaCl, 5% (vol/vol) glycerol, 1 mM L-serine (ACROS Organics), 1% DDM and 0.1% CHS (Anatrace)) and stirring for 1 h at 4 °C. The sample was ultracentrifuged (236,000 g, 30 min, 4 °C) to remove unsolubilized particles. The supernatant was incubated for 1 h at 4 °C while gently rocking with Ni^{2+}-sepharose resin, column volume of 0.5 mL, which had been equilibrated with 10 times CV of Buffer D (50 mM Tris-HCl, pH 7.4, 250 mM NaCl, 40 mM Imidazole, 5% (vol/vol) glycerol, 1 mM L-serine (ACROS Organics), 0.02% DDM and 0.002% CHS (Anatrace)). Subsequently, the suspension was poured into a 10-ml disposable column (Bio-Rad). The unbound material was let to flow through, the column was washed with the Buffer D, and ASCT1 was eluted with Buffer E (50 mM Tris-HCl, pH 7.4, 250 mM NaCl, 500 mM Imidazole, 5% (vol/vol) glycerol, 1 mM L-serine (ACROS Organics), 0.02% DDM and 0.002% CHS (Anatrace)). Elution fraction was applied to size-exclusion chromatography column Superdex 200 10/300 (GE-Healthcare) that preliminarily was equilibrated with Buffer F (50 mM Tris-HCl, pH 7.4, 250 mM NaCl, 5% (vol/vol) glycerol, 1 mM L-serine (ACROS Organics), 0.02% DDM and 0.002% CHS (Anatrace)). Protein-containing fractions were used for reconstitution into proteoliposomes or concentrated with Vivaspin Turbo 4 (Sartorius) concentrator with 100 kDa cutoff size for the following preparation for Cryo-EM data collection.

2.3. Reconstitution into proteoliposomes

To reconstitute the proteins into liposomes, we used a mixture of *Escherichia coli* lipids and phosphatidylcholine in a ratio of 3:1 that additionally contained 5% (wt/wt) or 10% (wt/wt) cholesterol (Avanti Polar lipids) in indicated experiments. An aliquot of the liposome mixture was thawed and extruded through a 400-nm-diameter polycarbonate filter (Avestin) and afterward diluted with Buffer G (20 mM Tris-HCl, pH 7.0) to the final concentration of 4 mg ml^{-1}. Further, the mixture was destabilized with 10% Triton X-100 and fused with freshly purified wild-type or mutant ASCT1 in a ratio of 1:250 (protein/lipids). The mixture was nutated for 30 min at room temperature. Afterward, to remove detergent we added Bio-beads in four steps: first, add 25 mg ml^{-1} for 30 min at room temperature; second, add 15 mg ml^{-1} for 1 h at 4 °C; third, add 19 mg ml^{-1} with an overnight incubation at 4 °C; and lastly add 29 mg ml^{-1} for 2 h at 4 °C on the next morning. Proteoliposomes were isolated from the Bio-beads, collected by ultracentrifugation (443,000 g, 25 min, 4 °C), and resuspended into Buffer G to final concentration 20 mg ml^{-1}, aliquoted, flash frozen, and stored in liquid nitrogen.

2.4. Radiolabeled transport assays

For transport assays, an aliquot of proteoliposomes was thawed at room temperature with the following addition of 10 mM unlabeled L-serine or indicated L-amino acid and 50 mM NaCl. The resuspension was exposed to three cycles of freeze–thaw and extruded with 11 passages through 400-nm-diameter polycarbon-

ate filter (Avestin). The proteoliposomes were resuspended with Buffer G and ultracentrifuged (443,000 g, 25 min, 4 °C) to remove excess of the substrate and again resuspended in the Buffer G with final concentration 20 mg ml^{-1} that contains 10 μg of the protein in total. The assays were performed at a water bath with set 25 °C and stirring 200 rpm. The external buffer contains 50 mM NaCl, 50 μM non-radioactive amino acid of interest, 0.3 μM [^{14}C]L-amino acid (PerkinElmer), and 20 mM Tris-HCl, pH 7.0 in the total volume of 600 μL. As a start point, 80 μL of the external buffer was quenched (to stop transport) by 2 mL of cold Buffer G, and the proteoliposomes with 1.6 μg of protein were added and immediately filtered through 0.45 nm pore-size filter (Protran BA-85, Whatman) and the filter stored. To start the transport, the rest of the proteoliposomes that contain 8.4 μg of the protein were diluted in 520 μL of the external buffer. For each time point, 80 μL of the external buffer was quenched by 2 mL of cold Buffer G, filtered through 0.45 nm pore-size filter (Protran BA-85, Whatman), washed by another 2 mL of cold Buffer G and stored. After the last time point, three fresh filters were treated by 20 μL of the external buffer and stored for calculations of the total counts. After the experiment, the filters were dissolved in 2 mL filter count scintillation liquid (Emulsifier Scintillator Plus, PerkinElmer). The radioactivity of the filters was measured with a PerkinElmer Tri-Carb 2800 RT scintillation counter. Error bars are represented at least three independent experiments.

For experiments to test the electrogenic nature of the exchange, the proteoliposomes were loaded with 10 mM unlabeled L-serine (ACROS Organics) and 50 mM KCl or 50 mM NaCl for a negative control. During the experiment, the external buffer was additionally supplied with 3 μM valinomycin at indicated time points. The assays were performed as described above.

For the competition transport assays the proteoliposomes were loaded with 10 mM unlabeled L-serine (ACROS Organics) and 50 mM NaCl. The external buffer for the assays was additionally supplied with 1 mM of the indicated unlabeled amino acid, 50 mM NaCl, 0.3 μM [^{14}C]L-serine (PerkinElmer), and 20 mM Tris-HCl, pH 7.0. After 30 min of the exchange the aliquots of data points were collected identically to the competition transport assays.

For the exchange transport assays the proteoliposomes were loaded with 10 mM unlabeled indicated amino acid and 50 mM NaCl. The external buffer contains 50 mM NaCl, 50 μM non-radioactive L-serine, 0.3 μM [^{14}C]L-serine (PerkinElmer), and 20 mM Tris-HCl, pH 7.0 After 30 min of the exchange the aliquots of data points were collected identically to the competition transport assays.

2.5. Cryo-EM sample preparation, imaging and data processing

For cryo-EM sample preparation, 3 μL of concentrated sample at ~ 8 mg/ml (100 kDa cut-off, Amicon), was applied to freshly glow-discharged (easiGlo Ted Pella, 20 mA, 40 s) grids (Quantifoil Au 1.2/1.3 200 mesh), blotted and plunge frozen in liquid ethane using a Leica GP2 plunger. Data collection was carried on a Titan Krios (Thermo Fisher Scientific) equipped with a K3 direct-electron detector (Gatan). SerialEM [50] was used for automated data collection, using an image-shift based (9 holes) procedure, with a defocus range of −1.0 to −2.0 μm and a dose rate of 15 e^-/px/s and a pixel size of 0.8521 A. Micrographs were collected with 50 ms exposure per frame for a total of 3 s, resulting in 60 frames total. Data processing was carried out using established protocols, as part of the software packages RELION [51] (version 3.1.2) and cryoSPARC (v3.2.0). A total of 4899 micrographs were subjected to motion correction (MotionCor2 [52]) and CTF estimation using CTFFIND4 [53], followed by reference-free and reference-based particle picking, 2D classification and final reconstruction in cryoSPARC using non-uniform refinement [54], while applying C3 symmetry, resulting in a map of 4.2 Å resolution (FSC = 0.143). All attempts to reconstruct in C1 resulted in maps of lower resolution (~6 Å), while not showing any asymmetric features.

2.6. Model building and refinement

As a starting model we used ASCT2 structure (PDB ID 6GCT), which was manually adjusted in Coot to match the sequence of ASCT1 and fit the density. Real space refinement and validation was done in Phenix.

2.7. Molecular dynamics simulations

We performed atomistic MD simulations of the obtained cryo-EM structure of ASCT1 wild-type (WT) and in-silico designed mutants (E256K, G381R, R457W) embedded in a lipid membrane in aqueous salt solutions. All MD simulations were performed using the MD package Gromacs (version 2018.1) [55] and the CHARMM36 force field [56–58]. The membrane builder tool of the CHARMM-GUI [59,60] (http://www.charmm-gui.org/?doc = input/membrane.bilayer) was used to embed the protein structure in a rectangular lipid bilayer composed of a mixture of 400 molecules of 1-palmitoyl-2-oleoyl-*sn*-glycero-3-phosphoethanolamine (POPE), 1-palmitoyl-2-oleoyl-*sn*-glycero-3-phosphoglycerol (POPG) and 1-palmitoyl-2-oleoyl-*sn*-glycero-3-phosphocholine (POPC) lipids in the ratio 3:3:2 as was used in the proteoliposomes in our *in-vitro* experiments and solvated with 150 mM aqueous NaCl solution. The box dimensions of the system were 130 × 130 × 130 Å. The system was then solvated with TIP3P water molecules [61] such that every protein atom was at least 12 Å away from the side of the box. Periodic boundary conditions were employed and the particle-mesh Ewald method [62,63] was used for treatment of long-range electrostatic interactions. The systems were optimized and equilibrated for 1 ns in the NVT ensemble and 20 ns in the NPT ensemble. After the equilibration stages, a 1 μs long unrestrained run was carried out for each system. The pressure was maintained at 1 atm semi-isotropically with the Parinello–Rahman barostat [64,65] and a coupling constant of 1.0 ps. The simulations were conducted at a constant temperature of 303.15 K using the Nosé-Hoover thermostat [66,67]. The total number of atoms in the simulation box was ~ 230 000 atoms. Visual inspection of the trajectories was performed with VMD [68] and the open source version of PyMOL.

3. Results

3.1. Functional characterization

We expressed unmodified human ASCT1 (SLC1A4) as well as two mutant forms (E256K and R457W) in the yeast *Pichia pastoris*, and purified it by combination of immobilized metal affinity and size exclusion chromatography (Supplementary Fig. 1). To test that the WT protein is functional, we reconstituted the protein into proteoliposomes (according to the published protocol [69]) and performed transport assays. Reconstituted ASCT1 readily transports radioactive L-Ser and L-Ala but it does not transport L-Gln (Fig. 1a, c, e). Interestingly, the uptake of L-Ser is inversely correlated to the cholesterol content in the proteoliposomes – the increase of cholesterol from 0 to 10% leads to more than 2-fold decrease in the substrate uptake (Fig. 1a). Similarly to ASCT2 [14], using our experimental setup, the exchange of amino acid pools via ASCT1 seems to be electroneutral as an addition of valinomycin showed no effect on the transport (Fig. 1b).

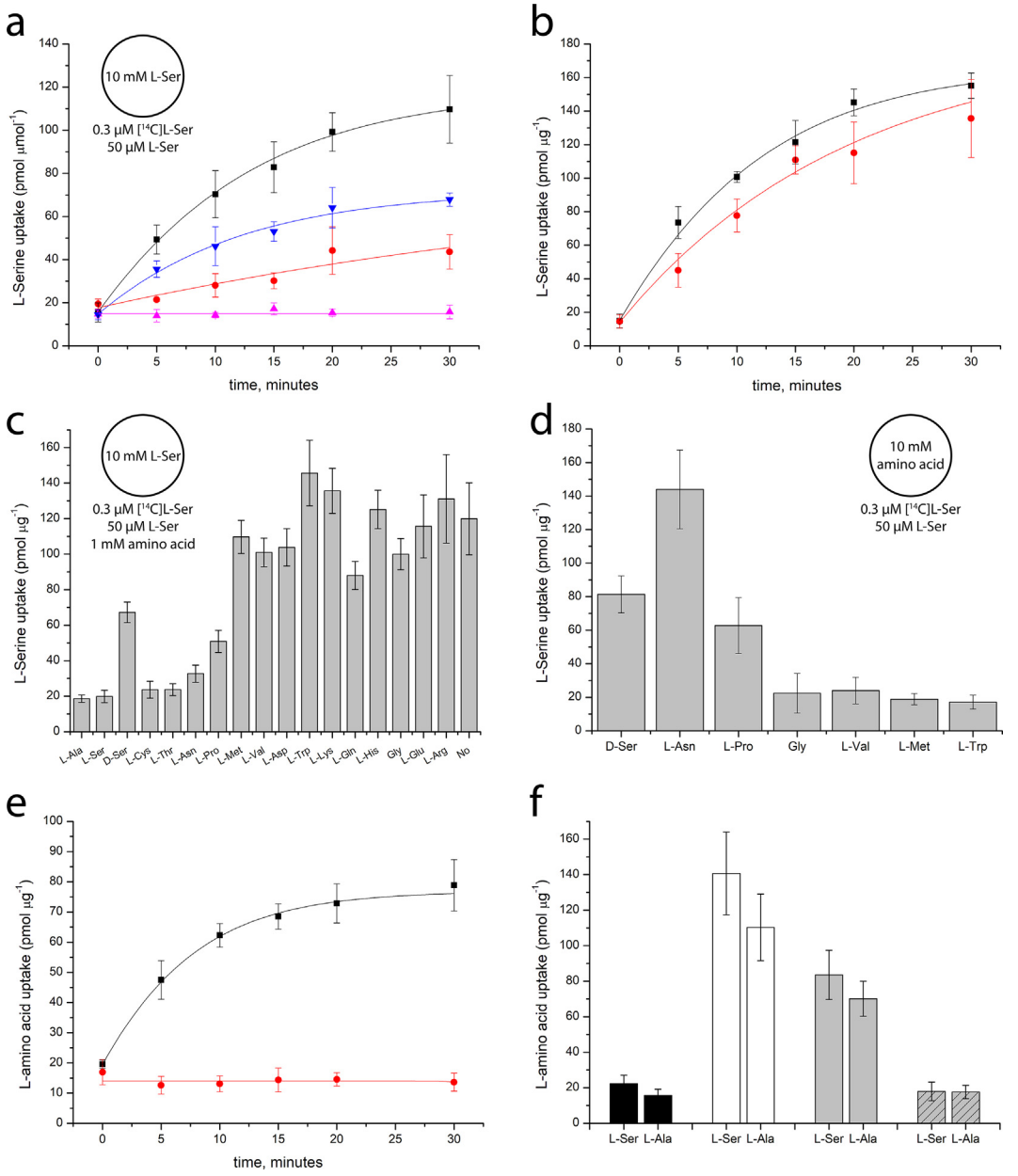

Fig. 1. Functional characterization of ASCT1 (a) Exchange of internal unlabeled L-serine with external [^{14}C]L-serine in proteoliposomes with different amounts of cholesterol. Black squares - proteoliposomes without added cholesterol; blue downward triangles - with 5% (wt/wt) cholesterol; red circles - with 10% (wt/wt) cholesterol, pink triangles – empty (no substrate inside) proteoliposomes. (**b)** Electroneutral nature of exchange and sodium dependency. Black squares – 3 μM valinomycin was added at the start to proteoliposomes, loaded with 50 mM KCl; red circles – 3 μM valinomycin was added at 14 min to proteoliposomes, loaded with 50 mM KCl. (**c)** Impact of a second unlabeled amino acid in excess, indicated in x-axis on [^{14}C]L-serine uptake. (**d)** Exchange of internal unlabeled amino acid, indicated in x-axis, with external [^{14}C]L-serine in proteoliposomes. (**e)** Exchange of external radioactive amino acid in proteoliposomes. Black – exchange of internal unlabeled L-alanine with external [^{14}C]L-alanine; red – exchange of internal unlabeled L-glutamine with external [^{3}H]L-glutamine. (**f**) Diminished uptake of radioactive L-serine and L-alanine – bars in black, white, gray, and slant gray for empty liposomes, WT, E256K and R457W mutants respectively. Data points and error bars represent means ± s.e.m. from three independent experiments, each done in at least two technical replicates. (For interpretation of the references to colour in this figure legend, the reader is referred to the web version of this article.)

Furthermore, we tested substrate specificity of ASCT1 with the following setups: (i) we monitored the uptake of radioactive L-Ser into the proteoliposomes in the 1 mM excess of an amino acid in the outside buffer ('inward competition'); and (ii) with the 10 mM excess of an amino acid inside proteoliposomes ('outward competition'). We observed the significant decrease in the uptake of radioactive L-Ser in the presence of L-Ala, L-Cys, L-Thr and L-Asn, and the moderate decrease in the presence of D-Ser and L-Pro (Fig. 1c). The presence of L-Met, L-Val, L-Asp, L-Gln, L-Trp, L-Lys and Gly did not affect the uptake of radioactive L-Ser. In the setup (ii), we observed the uptake of the radioactive L-Ser into proteoliposomes, indicating that indeed an exchange of L-Asn, L-Pro, and D-Ser trapped inside the proteoliposomes with the external substrate has taken place (Fig. 1d), but we observed no exchange of internal unlabeled L-Gln with external [^{3}H]L-Gln (Fig. 1e). The introduced point mutations were detrimental for the substrate uptake (Fig. 1f and §3.3).

3.2. Structure of ASCT1

We solved the structure of human ASCT1 incorporated into the n-dodecyl-β-D-maltopyranoside (DDM) micelles using single

particle cryo-EM technique at the overall resolution of 4.2 Å (Table 1, Supplementary Fig. 2). ASCT1 shares over 56% sequence identity with ASCT2 and as all other members of SLC1 family characterized up to date [14,70–72] it forms a homotrimer (Fig. 2a), with the core scaffold domain (TMS 1, 2, 4, and 5) and three independent transport ('elevator') domains (TMS 3, 6, 7, and 8) (Fig. 2c). Two pseudosymmetrical helical hairpins (HP1 and HP2) between TM6 and TM8 shield the binding site (Fig. 2b,c), although only HP2 was shown to be a gate both in inward and outward conformations of ASCT2 [72,73]. The quality of the density was sufficient to build a model for the most of the protein, except for the flexible loops connecting transport domains to the scaffold domains (3–4 loop between TMS3 and 4) and N- and C-termini (residues 1–37 and 482–532 respectively), which are predicted to be disordered (Supplementary Fig. 3). The transport domains are parked in the inward orientation and are detached from the scaffold in a similar fashion as observed in ASCT2 [14] (rmsd ~ 2 Å). ASCT1 also possesses a docking platform for the envelope proteins of retroviral origin, which protrudes in the extracellular space and is formed by a long (~35 amino acid) loop between segments of TM4 (Fig. 2a, e), which folds into an antiparallel β-strand. This antenna-like stem is only partially conserved (Fig. 2e) and is longer than in ASCT2 with an additional insert of five amino acids, namely Asn-Ser-Ser-Ser-Gly. Asn201 of this insertion as well as Asn206 just right after the insert are known to be glycosylated, which possibly is exploited by envelope proteins as the recognition pattern.

The substrate binding site of ASCT1 is nearly identical to the one in ASCT2 (Fig. 2b, d), albeit with one important substitution of C467 (ASCT2 numbering) to T459 (ASCT1 numbering). This is a key residue for the substrate selectivity; in EAATs it is invariantly an arginine residue, which allows binding of acidic substrates such as aspartate and glutamate [70]. In both ASCT1 and ASCT2 the binding cavity is negatively charged (Supplementary Fig. 4), hence impeding the binding of glutamate and aspartate, whereas the geometry of cavity restricts the entry of positively charged lysine, arginine and histidine. Unfortunately, it was not possible to assign the bound substrate due to the limited resolution, therefore the direct comparison of substrate binding modes currently is not possible. Nevertheless, MD simulations indicate that the binding modes are likely to be very similar (Supplementary Fig. 5).

At the obtained resolution it is also impossible to assign sodium ions. However, taking into account the conservation of the binding sites in the SLC1 family, positions of sodium ions in archaeal homolog Glt_{Tk} [74] as well as results of MD simulations performed earlier for ASCT2 [75], the most probable sodium binding residues in ASCT1 are as follows: site 1 – E465, D467; site 2 – T376, V418, and site 3 – F121, T124, T125, N378, D380 respectively (Fig. 2d). This is mostly in agreement with the recently proposed positions of sodium ions in ASCT1 based on homology modelling [17].

3.3. Impact of mutations

The resolution of the obtained reconstruction is sufficient to map the mutations shown to be disease-related (Fig. 3). Mutation of Glu256 to Lys (E256K) is known to reduce the uptake of substrates [46]. We performed the *in vitro* characterization of this mutant, which indeed revealed about 30–40% decrease in the uptake of radioactive L-Ser and L-Ala (Fig. 1f). Residue 256 is located at the base of the transporter, in the first part of the TM5 scaffold helix, and in the wildtype protein its side chain either interacts with the preceding Asn255 residue or is fully solvent exposed. This position is relatively far from the transport domains (~13 Å away from HP2), therefore it is hard to envision how substitution to Lys could affect the transport rates. Based on the obtained structure we can propose that Lys at this position can either (i) make a polar contact with Ser100 of TM2 scaffold helix which in turn interacts with TM3 of the transport domain; or (ii) make a salt bridge with Glu243 of TM5 of the neighboring protomer, which is in turn coordinates TM3 of the same neighboring protomer, or (iii) perhaps even attract and anchor HP2 as it was seen in ASCT2 that HP2 opens towards this part of the protein [73]. To check if any of these scenarios are possible, we performed all-atom MD simulations that confirmed the scenario (ii) – we observed the formation of Lys256-Glu243′ (′ stands for an adjacent protomer) salt bridge, which remained stable over 400 ns of simulation time (Supplementary Figs. 6, 9–10).

Another well characterized mutation is R457W and it leads to the complete loss of substrate uptake [46]. We were able to reproduce this result in our experimental setup, where the uptake of radioactive substrates was at the level of empty liposomes (Fig. 1f). R457 of TM8 of the transport domain is located nearby the substrate binding site and somewhat sits in-between HP1 and HP2 elements. Judging from this location, introduction of the bulky sidechain at this position might interfere with the normal function of the gate, securing the substrate site, hence probably preventing substrate loading or discharge. MD simulations revealed a peculiar arrangement, where W457 side chain forms a stable S-π interaction [76] with the side chain of Cys343 (Supplementary Figs. 7, 9–10), hence anchoring HP1 and pulling TMS8 out of this position. This is accompanied by the significant opening of HP2, which moves ~ 7 Å towards the scaffold domain (Supplementary Fig. 7).

There is another rare mutation characterized recently, namely G381R. This residue sits in the essentially conserved Asn-Met-Asp-Gly motif of TMS7, known to play an important role in the formation of sodium binding sites and coupling of sodium and substrate binding [74,77]. Intriguingly, at this position the closest interaction of TMS7 and TMS8 is observed, hence the replacement of Gly to Arg must have very dramatic consequences, leading to the distortion of both cation and substrate binding sites, thus rendering transporter to be non-functional. MD simulations revealed a significant effect of the G381R mutation on the entire substrate-binding pocket, causing destabilization of the helices in the

Table 1
Cryo-EM data collection, refinement and validation statistics.

Data collection and processing	
Magnification	29,000
Voltage (kV)	300
Electron exposure (e^{-}/Å^2)	60
Defocus range (μm)	−1.0 – −2.0
Pixel size (Å)	0.8521
Symmetry imposed	C3
Initial particle images (no.)	1,336,001
Final particle images (no.)	134,344
Map resolution (Å) FSC = 0.143	4.2
Refinement	
Initial model	PDB 6GCT
Model composition	
Nonhydrogen atoms	9510
Protein residues	1284
R.m.s. deviations	
Bond lengths (Å)	0.003
Bond angles (°)	0.69
Validation	
MolProbity score	1.96
Clashscore	11.6
Poor rotamers (%)	0.0
Ramachandran plot	
Favored (%)	94.34
Allowed (%)	5.66
Disallowed (%)	0.00
CC_mask	0.84
CC_volume	0.83

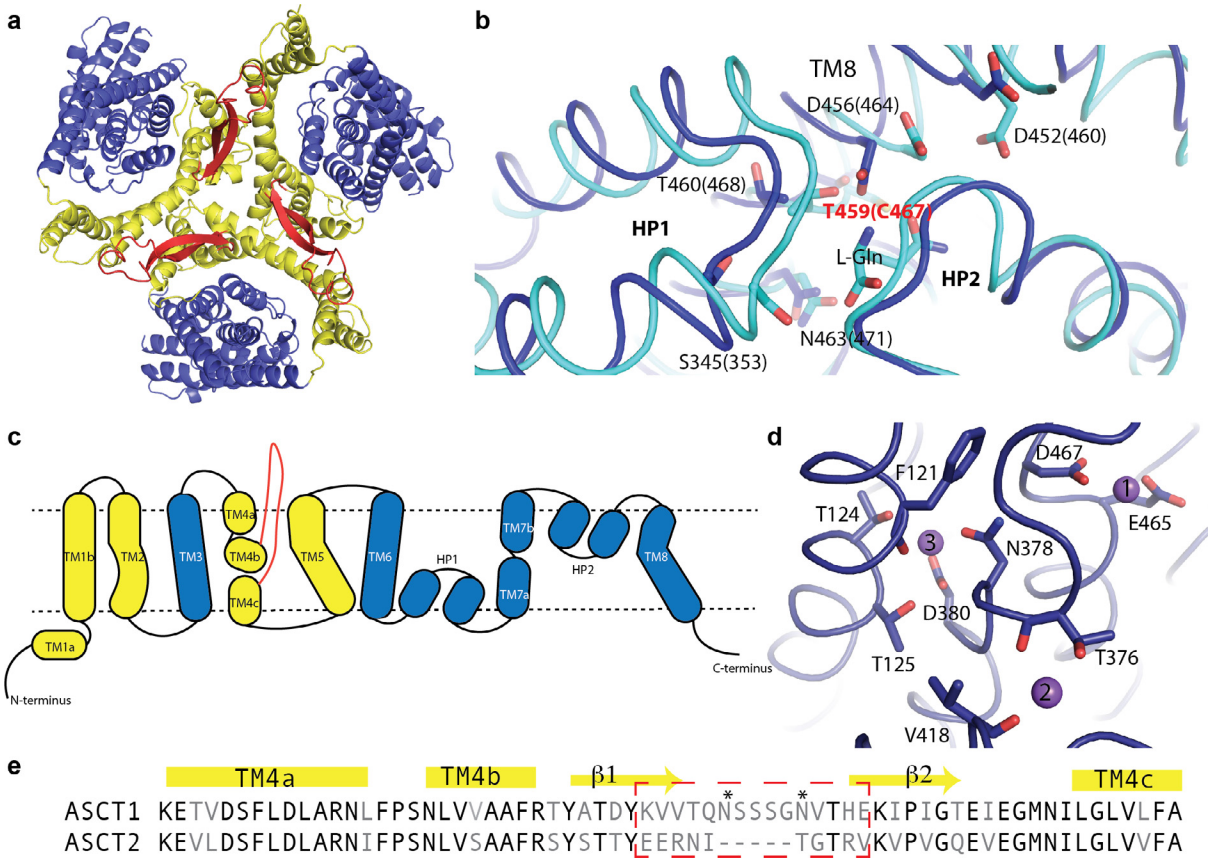

Fig. 2. Structure of ASCT1 (a) Top view onto ASCT1 trimer (shown as cartoon). Scaffold and transport domains in yellow and blue respectively, extracellular extensions in red. **(b)** Superposition of binding sites between ASCT1 (blue) and ASCT2 (cyan). The main residues involved are shown as sticks and numbered (in parentheses numbering for ASCT2). The only substitution is indicated with red. **(c)** The secondary structure diagram, coloring as in panel **a**. (**d**) Predicted positions of sodium (purple spheres) in ASCT1. **(e)** The sequence alignment around the extracellular extension region. Non-identical amino acids indicated with grey. The highly variable part is within the red dashed rectangle. N-glycosylated residues marked with an *. (For interpretation of the references to colour in this figure legend, the reader is referred to the web version of this article.)

ligand-binding site and rearrangement of the HP1 and HP2 loops (Supplementary Figs. 8–10). Such deformations seem not to be compatible with the normal ASCT1 function [49]. This might be also the reason why we failed to produce this mutant.

4. Discussion

In here presented structure of ASCT1 extends the number of structurally characterized members of the SLC1 family, with structures available for ASCT2 [14,72], EAAT1 [70] and EAAT3 [71]. All of these reported structures are very similar in general – arranged in trimers with the scaffold domains making a core with the transport domains at the periphery, which is also reflected in a highly conserved transport mechanism, described as a one-gate elevator movement across the membrane. Still there is a number of major differences between the two subfamilies. ASCT proteins have a long insertion in-between segments of TMS4, which forms a so-called docking platform made of three (one from each protomer) β-hairpins with the extended loops, decorated by glycosylation. This platform can be recognized by the envelope proteins of endo- or exogenous retroviruses [78,79], which ultimately leads to the membrane (and cell) fusion. In humans such interactions are essential during the placenta formation [80], and occur between a product of Human Endogenous Retrovirus Group W family 1 member, also termed syncytin-1, and ASCT1 and ASCT2 proteins, at least *in vitro* [79].

The other distinct feature of ASCT proteins compared to EAATs is that the former perform the exchange of neutral amino acids, whereas the latter are capable to concentrate acidic amino acids against the gradient. This implies that the substrate transport in EAATs is unidirectional, and ASCTs perform equilibration of the amino acid pools, therefore it is quite likely that ASCTs should not have any *apo*-states. That would also mean that the sodium-substrate coupling mechanism described for EAATs and archaeal homologues, should not be applicable to ASCTs. However the analysis of the differences in the ion coupling have to be postponed until higher resolution structures are obtained.

As seen from the analysis of binding sites, the substrate specificity is dictated by the charge of a cavity, which selects for negatively charged (EAATs) or neutral (ASCTs) substrates and by its geometry, which excludes the access of the bulky amino acids. ASCT1 and ASCT2 have overlapping substrate specificities, albeit ASCT1 cannot transport glutamine [27], (Fig. 1), which perhaps is caused by a narrower binding site (Supplementary Fig. 4), but it can accommodate (hydroxy)-proline, which is readily transported [27,41], (Fig. 1). The emerging picture that despite L- and D-Ser are substrates of both ASCT1 and ASCT2, the former might be the main serine transporter in the brain [39]. It must be noted though, that there is no real consensus whether there is indeed preferential expression of ASCT1 in astrocytes and of ASCT2 in neurons, as results are contradictory and vary with the different experimental techniques [18,81–84].

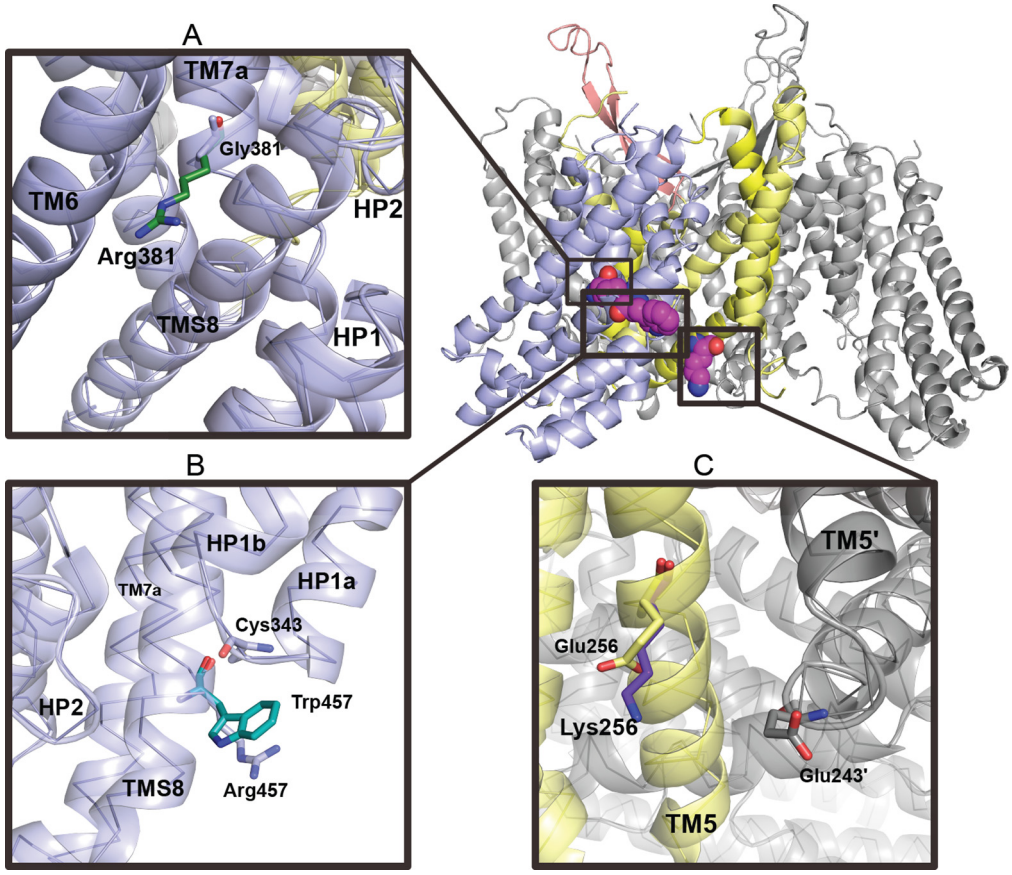

Fig. 3. Disease-linked mutations in ASCT1 (**a**) G381R (**b**) R457W (**c**) E256K. The scaffold and transport domains in pale yellow and pale blue respectively. Upper right panel shows global positions of affected residues, shown with magenta spheres. See also Supplementary Figures 6–10. (For interpretation of the references to colour in this figure legend, the reader is referred to the web version of this article.)

It is puzzling, that the transport in ASCT1 is negatively affected by cholesterol (Fig. 1), although previously we observed the opposite effect for ASCT2, where 10% of added cholesterol led to twice the amount of transported substrate [14]. In the adult brain, the majority of cholesterol is synthesized in the astrocytes, which is redistributed to neurons [85], and the cholesterol content in the plasma membranes of the latter is about twice less [86]. Whether there is a real correlation between the cholesterol content in the membrane, localization of a transporter and its kinetics remains to be explored, preferably using systems better mimicking the lipid composition of human cells.

Mutations profiled in ASCT1 further support the idea of its major role in the transport of D-Ser and neurodevelopment. Malfunctioning of ASCT1 leads to early developmental delays, spastic tetraplegia, thin corpus callosum, and progressive microcephaly [44,46–48]. The carriers unable to develop motor skills for independent walking, typically unable to speak and have severe intellectual disability. Importantly these conditions appear even if ASCT2 is intact. And as seen from our functional characterization – E256K leads to the diminished exchange of substrates, whereas R457W completely abolishes the transport (Fig. 1f).

MD simulations further corroborate that the characterized mutations might either interfere with the movements of a transport domain (E256K) or disturb the loading / unloading of a substrate (R457W). The third point mutation G381R is very destabilizing and leads to the collapse of the binding site.

To summarize, our data confirm that ASCT1 is a neutral amino acid exchanger with the preference for Ala, Cys, Thr, Asn, Pro and both L- and D-Ser. The obtained structure is instrumental to map the point mutations in ASCT1, our functional analysis confirms the impact of mutations on the transport activity and MD simulations explain how these mutations hinder the transport of substrates.

CRediT authorship contribution statement

Pavlo Stehantsev: Investigation, Visualization. **Artem Stetsenko:** Investigation, Visualization, Writing – original draft. **Mariia Nemchinova:** Investigation, Visualization. **Nanda Gowtham Aduri:** Investigation, Visualization. **Siewert J. Marrink:** Methodology, Supervision. **Cornelius Gati:** Methodology, Visualization, Supervision. **Albert Guskov:** Conceptualization, Methodology, Visualization, Writing – original draft, Writing – review & editing.

Acknowledgments

We thank Dirk J. Slotboom for discussions related to this manuscript.

Funding

Dutch Scientific Organization NWO, OCENW.KLEIN.141 (AG).

Data and materials availability

Atomic coordinates and the corresponding electron microscopy density map are deposited in the Protein Data Bank and the Elec-

tron Microscopy Data Bank under accession number 7P4I and EMD-13193, respectively. Models and parameter files used for MD simulations are freely available from the Zenodo website at the following url https://doi.org/10.5281/zenodo.5092014.

Appendix A. Supplementary data

Supplementary data to this article can be found online at https://doi.org/10.1016/j.csbj.2021.09.015.

References

[1] Kanai Y, Hediger MA. The glutamate/neutral amino acid transporter family SLC1: Molecular, physiological and pharmacological aspects. Pflugers Arch. Eur. J. Physiol. 2004;447(5):469–79. https://doi.org/10.1007/s00424-003-1146-4.

[2] Kanai Y et al. The SLC1 high-affinity glutamate and neutral amino acid transporter family. Mol. Aspects Med. 2013;34(2–3):108–20. https://doi.org/10.1016/j.mam.2013.01.001.

[3] Grewer C, Gameiro A, Rauen T. SLC1 glutamate transporters. Pflugers Arch. Eur. J. Physiol. 2014;466(1):3–24. https://doi.org/10.1007/s00424-013-1397-7.

[4] Kanner BI, Sharon I. Active Transport of L-Glutamate by Membrane Vesicles Isolated from Rat Brain. Biochemistry 1978;17(19):3949–53. https://doi.org/10.1021/bi00612a011.

[5] Zerangue N, Kavanaugh MP. Flux coupling in a neuronal glutamate transporter. Nature 1996;383(6601):634–7. https://doi.org/10.1038/383634a0.

[6] J. Rothstein et al., "Antisense knockout of glutamate transporters reveals a predominant role for astroglial glutamate transport in excitotoxicity and clearance of extracellular glutamate," Neuron, vol. 16, pp. 675–686, 1996, [Online]. Available: papers2://publication/uuid/327F682D-2D03-48C7-A0E6-A57E2CD92157.

[7] Zhang Y, Bendahan A, Zarbiv R, Kavanaugh MP, Kanner BI. Molecular determinant of ion selectivity of a (Na+ + K+)-coupled rat brain glutamate transporter. Proc. Natl. Acad. Sci. U. S. A. 1998;95(2):751–5. https://doi.org/10.1073/pnas.95.2.751.

[8] Pines G, Kanner BI. Counterflow of L-glutamate in plasma membrane vesicles and reconstituted preparations from rat brain. Biochemistry 1990;29(51):11209–14. https://doi.org/10.1021/bi00503a008.

[9] Arriza JL, Eliasof S, Kavanaugh MP, Amara SG. Excitatory amino acid transporter 5, a retinal glutamate transporter coupled to a chloride conductance. Proc. Natl. Acad. Sci. U. S. A. 1997;94(8):4155–60. https://doi.org/10.1073/pnas.94.8.4155.

[10] Utsunomiya-Tate N, Endou H, Kanai Y. Cloning and functional characterization of a system ASC-like Na+-dependent neutral amino acid transporter. J. Biol. Chem. 1996;271(25):14883–90. https://doi.org/10.1074/jbc.271.25.14883.

[11] Leary GP, Stone EF, Holley DC, Kavanaugh MP. The glutamate and chloride permeation pathways are colocalized in individual neuronal glutamate transporter subunits. J. Neurosci. 2007;27(11):2938–42. https://doi.org/10.1523/JNEUROSCI.4851-06.2007.

[12] Wadiche JI, Amara SG, Kavanaugh MP. Ion fluxes associated with excitatory amino acid transport. Neuron 1995;15(3):721–8. https://doi.org/10.1016/0896-6273(95)90159-0.

[13] Billups B, Rossi D, Attwell D. Anion conductance behavior of the glutamate uptake carrier in salamander retinal glial cells. J. Neurosci. 1996;16(21):6722–31. https://doi.org/10.1523/jneurosci.16-21-06722.1996.

[14] Garaeva AA, Oostergetel GT, Gati C, Guskov A, Paulino C, Slotboom DJ. Cryo-EM structure of the human neutral amino acid transporter ASCT2. Nat. Struct. Mol. Biol. 2018;25(6):515–21. https://doi.org/10.1038/s41594-018-0076-y.

[15] Bröer A, Wagner C, Lang F, Bröer S. Neutral amino acid transporter ASCT2 displays substrate-induced Na+ exchange and a substrate-gated anion conductance. Biochem. J. 2000;346(3):705–10. https://doi.org/10.1042/0264-6021:3460705.

[16] Zerangue N, Kavanaugh MP. ASCT-1 is a neutral amino acid exchanger with chloride channel activity. J. Biol. Chem. 1996;271(45):27991–4. https://doi.org/10.1074/jbc.271.45.27991.

[17] Scalise M, Console L, Cosco J, Pochini L, Galluccio M, Indiveri C. ASCT1 and ASCT2: Brother and Sister? SLAS Discov. 2021. https://doi.org/10.1177/24725552211030288.

[18] Sakai K, Shimizu H, Koike T, Furuya S, Watanabe M. Neutral amino acid transporter ASCT1 is preferentially expressed in L-Ser-synthetic/storing glial cells in the mouse brain with transient expression in developing capillaries. J. Neurosci. 2003;23(2):550–60. https://doi.org/10.1523/jneurosci.23-02-00550.2003.

[19] Arriza JL et al. Cloning and expression of a human neutral amino acid transporter with structural similarity to the glutamate transporter gene family. J. Biol. Chem. 1993;268(21):15329–32. https://doi.org/10.1016/s0021-9258(18)82257-8.

[20] Shafgat S et al. Cloning and expression of a novel Na+-dependent neutral amino acid transporter structurally related to mammalian Na+/glutamate cotransporters. J. Biol. Chem. 1993;268(21):15351–5. https://doi.org/10.1016/s0021-9258(18)82263-3.

[21] Hediger MA, Clémençon B, Burrier RE, Bruford EA. The ABCs of membrane transporters in health and disease (SLC series): Introduction. Mol. Aspects Med. 2013;34(2–3):95–107. https://doi.org/10.1016/j.mam.2012.12.009.

[22] Jiang H, Zhang N, Tang T, Feng F, Sun H, Qu W. Target the human Alanine/Serine/Cysteine Transporter 2(ASCT2): Achievement and Future for Novel Cancer Therapy. Pharmacol. Res. 2020;vol. 158, no. May:. https://doi.org/10.1016/j.phrs.2020.104844104844.

[23] Scalise M, Pochini L, Galluccio M, Console L, Indiveri C. Glutamine transport and mitochondrial metabolism in cancer cell growth. Front. Oncol. 2017;7(DEC):1–9. https://doi.org/10.3389/fonc.2017.00306.

[24] DeBerardinis RJ et al. Beyond aerobic glycolysis: Transformed cells can engage in glutamine metabolism that exceeds the requirement for protein and nucleotide synthesis. Proc. Natl. Acad. Sci. U. S. A. 2007;104(49):19345–50. https://doi.org/10.1073/pnas.0709747104.

[25] Younes M, Pathak M, Finnie D, Sifers RN, Liu Y, Schwartz MR. Expression of the neutral amino acids transporter ASCT1 in esophageal carcinomas. Anticancer Res. 2000;20(5C):3775–9.

[26] Wang Q et al. Targeting amino acid transport in metastatic castration-resistant prostate cancer: Effects on cell cycle, cell growth, and tumor development. J. Natl. Cancer Inst. 2013;105(19):1463–73. https://doi.org/10.1093/jnci/djt241.

[27] Pinilla-Tenas J, Barber A, Lostao MP. Transport of proline and hydroxyproline by the neutral amino-acid exchanger ASCT1. J. Membr. Biol. 2003;195(1):27–32. https://doi.org/10.1007/s00232-003-2041-9.

[28] Yang JH et al. Brain-specific Phgdh deletion reveals a pivotal role for l-serine biosynthesis in controlling the level of D-serine, an N-methyl-D-aspartate receptor co-agonist, in adult brain. J. Biol. Chem. 2010;285(53):41380–90. https://doi.org/10.1074/jbc.M110.187443.

[29] Schell MJ, Molliver ME, Snyder SH. D-serine, an endogenous synaptic modulator: Localization to astrocytes and glutamate-stimulated release. Proc. Natl. Acad. Sci. U. S. A. 1995;92(9):3948–52. https://doi.org/10.1073/pnas.92.9.3948.

[30] Radzishevsky I, Sason H, Wolosker H. D-Serine: Physiology and pathology. Curr. Opin. Clin. Nutr. Metab. Care 2013;16(1):72–5. https://doi.org/10.1097/MCO.0b013e32835a3466.

[31] Hashimoto A, Nishikawa T, Oka T, Takahashi K. Endogenous d-Serine in Rat Brain: N-Methyl-d-Aspartate Receptor-Related Distribution and Aging. J. Neurochem. 1993;60(2):783–6. https://doi.org/10.1111/j.1471-4159.1993.tb03219.x.

[32] Mothet JP et al. D-serine is an endogenous ligand for the glycine site of the N-methyl-D-aspartate receptor. Proc. Natl. Acad. Sci. U. S. A. 2000;97(9):4926–31. https://doi.org/10.1073/pnas.97.9.4926.

[33] Wolosker H, Blackshaw S, Snyder SH. Serine racemase: A glial enzyme synthesizing D-serine to regulate glutamate-N-methyl-D-aspartate neurotransmission. Proc. Natl. Acad. Sci. U. S. A. 1999;96(23):13409–14. https://doi.org/10.1073/pnas.96.23.13409.

[34] Miya K et al. Serine racemase is predominantly localized in neurons in mouse brain. J. Comp. Neurol. 2008;510(6):641–54. https://doi.org/10.1002/cne.21822.

[35] Ehmsen JT et al. D-serine in glia and neurons derives from 3-phosphoglycerate dehydrogenase. J. Neurosci. 2013;33(30):12464–9. https://doi.org/10.1523/JNEUROSCI.4914-12.2013.

[36] Benneyworth MA, Li Y, Basu AC, Bolshakov VY, Coyle JT. Cell selective conditional null mutations of serine racemase demonstrate a predominate localization in cortical glutamatergic neurons. Cell. Mol. Neurobiol. 2012;32(4):613–24. https://doi.org/10.1007/s10571-012-9808-4.

[37] Yamasaki M, Yamada K, Furuya S, Mitoma J, Hirabayashi Y, Watanabe M. 3-Phosphoglycerate dehydrogenase, a key enzyme for L-serine biosynthesis, is preferentially expressed in the radial glia/astrocyte lineage and olfactory ensheathing glia in the mouse brain. J. Neurosci. 2001;21(19):7691–704. https://doi.org/10.1523/jneurosci.21-19-07691.2001.

[38] Wolosker H. Serine racemase and the serine shuttle between neurons and astrocytes. Biochim. Biophys. Acta - Proteins Proteomics 2011;1814(11):1558–66. https://doi.org/10.1016/j.bbapap.2011.01.001.

[39] Kaplan E et al. ASCT1 (Slc1a4) transporter is a physiologic regulator of brain D-serine and neurodevelopment. Proc. Natl. Acad. Sci. U. S. A. 2018;115(38):9628–33. https://doi.org/10.1073/pnas.1722677115.

[40] Kasai Y, Tachikawa M, Hirose S, Akanuma SI, Hosoya KI. Transport systems of serine at the brain barriers and in brain parenchymal cells. J. Neurochem. 2011;118(2):304–13. https://doi.org/10.1111/j.1471-4159.2011.07313.x.

[41] Foster AC et al. D-serine is a substrate for neutral amino acid transporters ASCT1/SLC1A4 and ASCT2/SLC1A5, and is transported by both subtypes in rat hippocampal astrocyte cultures. PLoS One 2016;11(6):1–18. https://doi.org/10.1371/journal.pone.0156551.

[42] Gliddon CM, Shao Z, LeMaistre JL, Anderson CM. Cellular distribution of the neutral amino acid transporter subtype ASCT2 in mouse brain. J. Neurochem. 2009;108(2):372–83. https://doi.org/10.1111/j.1471-4159.2008.05767.x.

[43] Bhat S, El-Kasaby A, Freissmuth M, Sucic S. Functional and Biochemical Consequences of Disease Variants in Neurotransmitter Transporters: A Special Emphasis on Folding and Trafficking Deficits. Pharmacol. Ther. 2021;222:. https://doi.org/10.1016/j.pharmthera.2020.107785107785.

[44] H.A. Abdelrahman, A. Al-Shamsi, A. John, B. R. Ali, L. Al-Gazali, "A Novel SLC1A4 Mutation (p.Y191*) Causes Spastic Tetraplegia, Thin Corpus Callosum, and Progressive Microcephaly (SPATCCM) With Seizure Disorder," Child Neurol. Open, vol. 6, p. 2329048X1988064, 2019, 10.1177/2329048x19880647.

[45] Conroy J et al. Novel European SLC1A4 variant: Infantile spasms and population ancestry analysis. J. Hum. Genet. 2016;61(8):761–4. https://doi.org/10.1038/jhg.2016.44.
[46] Damseh N et al. Mutations in SLC1A4, encoding the brain serine transporter, are associated with developmental delay, microcephaly and hypomyelination. J. Med. Genet. 2015;52(8):541–7. https://doi.org/10.1136/jmedgenet-2015-103104.
[47] Heimer G et al. SLC1A4 mutations cause a novel disorder of intellectual disability, progressive microcephaly, spasticity and thin corpus callosum. Clin. Genet. 2015;88(4):327–35. https://doi.org/10.1111/cge.12637.
[48] Srour M et al. A homozygous mutation in SLC1A4 in siblings with severe intellectual disability and microcephaly. Clin. Genet. 2015;88(1):E1–4. https://doi.org/10.1111/cge.12605.
[49] Pironti E et al. A novel SLC1A4 homozygous mutation causing congenital microcephaly, epileptic encephalopathy and spastic tetraparesis: a video-EEG and tractography–case study. J. Neurogenet. 2018;32(4):316–21. https://doi.org/10.1080/01677063.2018.1476510.
[50] Schorb M, Haberbosch I, Hagen WJH, Schwab Y, Mastronarde DN. Software tools for automated transmission electron microscopy. Nat. Methods 2019;16(6):471–7. https://doi.org/10.1038/s41592-019-0396-9.
[51] Scheres SHW. RELION: Implementation of a Bayesian approach to cryo-EM structure determination. J. Struct. Biol. 2012;180(3):519–30. https://doi.org/10.1016/j.jsb.2012.09.006.
[52] Zheng SQ, Palovcak E, Armache JP, Verba KA, Cheng Y, Agard DA. MotionCor2: Anisotropic correction of beam-induced motion for improved cryo-electron microscopy. Nat. Methods 2017;14(4):331–2. https://doi.org/10.1038/nmeth.4193.
[53] Rohou A, Grigorieff N. CTFFIND4: Fast and accurate defocus estimation from electron micrographs. J. Struct. Biol. 2015;192(2):216–21. https://doi.org/10.1016/j.jsb.2015.08.008.
[54] Punjani A, Zhang H, Fleet DJ. Non-uniform refinement: adaptive regularization improves single-particle cryo-EM reconstruction. Nat. Methods 2020;17(12):1214–21. https://doi.org/10.1038/s41592-020-00990-8.
[55] Abraham MJ et al. Gromacs: High performance molecular simulations through multi-level parallelism from laptops to supercomputers. SoftwareX 2015;1–2:19–25. https://doi.org/10.1016/j.softx.2015.06.001.
[56] Huang J, Mackerell AD. CHARMM36 all-atom additive protein force field: Validation based on comparison to NMR data. J. Comput. Chem. 2013;34(25):2135–45. https://doi.org/10.1002/jcc.23354.
[57] Klauda JB et al. Update of the CHARMM All-Atom Additive Force Field for Lipids: Validation on Six Lipid Types. J. Phys. Chem. B 2010;114(23):7830–43. https://doi.org/10.1021/jp101759q.
[58] Wu EL et al. CHARMM-GUI membrane builder toward realistic biological membrane simulations. J. Comput. Chem. 2014;35(27):1997–2004. https://doi.org/10.1002/jcc.23702.
[59] Lee J et al. CHARMM-GUI Input Generator for NAMD, GROMACS, AMBER, OpenMM, and CHARMM/OpenMM Simulations Using the CHARMM36 Additive Force Field. J. Chem. Theory Comput. 2016;12(1):405–13. https://doi.org/10.1021/acs.jctc.5b00935.
[60] Jo S, Kim T, Iyer VG, Im W. CHARMM-GUI: A web-based graphical user interface for CHARMM. J. Comput. Chem. 2008;29(11):1859–65. https://doi.org/10.1002/jcc.20945.
[61] Jorgensen WL, Chandrasekhar J, Madura JD, Impey RW, Klein ML. Comparison of simple potential functions for simulating liquid water. J. Chem. Phys. 1983;79(2):926–35. https://doi.org/10.1063/1.445869.
[62] Essmann U, Perera L, Berkowitz ML, Darden T, Lee H, Pedersen LG. A smooth particle mesh Ewald method. J. Chem. Phys. 1995;103(19):8577–93. https://doi.org/10.1063/1.470117.
[63] Darden T, York D, Pedersen L. Particle mesh Ewald: An N·log(N) method for Ewald sums in large systems. J. Chem. Phys. 1993;98(12):10089–92. https://doi.org/10.1063/1.464397.
[64] Parrinello M, Rahman A. Polymorphic transitions in single crystals: A new molecular dynamics method. J. Appl. Phys. 1981;52(12):7182–90. https://doi.org/10.1063/1.328693.
[65] Nosé S, Klein ML. Constant pressure molecular dynamics for molecular systems. Mol. Phys. 1983;50(5):1055–76. https://doi.org/10.1080/00268978300102851.
[66] Nosé S. A unified formulation of the constant temperature molecular dynamics methods. J. Chem. Phys. 1984;81(1):511–9. https://doi.org/10.1063/1.447334.
[67] Hoover WG. Canonical dynamics: Equilibrium phase-space distributions. Phys. Rev. A Mar. 1985;31(3):1695–7. https://doi.org/10.1103/PhysRevA.31.1695.
[68] Humphrey W, Dalke A, Schulten K. VMD: Visual molecular dynamics. J. Mol. Graph. Feb. 1996;14(1):33–8. https://doi.org/10.1016/0263-7855(96)00018-5.
[69] Geertsma ER, Nik Mahmood NAB, Schuurman-Wolters GK, Poolman B. Membrane reconstitution of ABC transporters and assays of translocator function. Nat. Protoc. 2008;3(2):256–66. https://doi.org/10.1038/nprot.2007.519.
[70] Canul-Tec JC et al. Structure and allosteric inhibition of excitatory amino acid transporter 1. Nature 2017;544(7651):446–51. https://doi.org/10.1038/nature22064.
[71] Qiu B, Matthies D, Fortea E, Yu Z, Boudker O. Cryo-EM structures of excitatory amino acid transporter 3 visualize coupled substrate, sodium, and proton binding and transport. Sci. Adv. 2021;7(10):1–10. https://doi.org/10.1126/sciadv.abf5814.
[72] Yu X et al. Cryo-EM structures of the human glutamine transporter SLC1a5 (ASCT2) in the outward-facing conformation. Elife 2019;8:1–17. https://doi.org/10.7554/eLife.48120.
[73] Garaeva AA, Guskov A, Slotboom DJ, Paulino C. A one-gate elevator mechanism for the human neutral amino acid transporter ASCT2. Nat. Commun. 2019;10(1):1–8. https://doi.org/10.1038/s41467-019-11363-x.
[74] Guskov A, Jensen S, Faustino I, Marrink SJ, Slotboom DJ. Coupled binding mechanism of three sodium ions and aspartate in the glutamate transporter homologue Glt Tk. Nat. Commun. 2016;7:1–6. https://doi.org/10.1038/ncomms13420.
[75] Zander CB, Albers T, Grewer C. Voltage-dependent processes in the electroneutral amino acid exchanger ASCT2. J. Gen. Physiol. 2013;141(6):659–72. https://doi.org/10.1085/jgp.201210948.
[76] Ringer AL, Senenko A, Sherrill CD. Models of S/π interactions in protein structures: Comparison of the H 2 S-benzene complex with PDB data. Protein Sci. 2007;16(10):2216–23. https://doi.org/10.1110/ps.073002307.
[77] Jensen S, Guskov A, Rempel S, Hänelt I, Slotboom DJ. Crystal structure of a substrate-free aspartate transporter. Nat. Struct. Mol. Biol. 2013;20(10):1224–7. https://doi.org/10.1038/nsmb.2663.
[78] Shimode S, Nakaoka R, Shogen H, Miyazawa T. Characterization of feline ASCT1 and ASCT2 as RD-114 virus receptor. J. Gen. Virol. 2013;94(PART7):1608–12. https://doi.org/10.1099/vir.0.052928-0.
[79] Lavillette D, Marin M, Ruggieri A, Mallet F, Cosset F-L, Kabat D. The Envelope Glycoprotein of Human Endogenous Retrovirus Type W Uses a Divergent Family of Amino Acid Transporters/Cell Surface Receptors. J. Virol. 2002;76(13):6442–52. https://doi.org/10.1128/jvi.76.13.6442-6452.2002.
[80] Roberts RM et al. Syncytins expressed in human placental trophoblast. Placenta 2021. https://doi.org/10.1016/j.placenta.2021.01.006.
[81] Weiss MD, Derazi S, Kilberg MS, Anderson KJ. Ontogeny and localization of the neutral amino acid transporter ASCT1 in rat brain. Dev. Brain Res. 2001;130(2):183–90. https://doi.org/10.1016/S0165-3806(01)00250-4.
[82] Bröer A et al. The astroglial ASCT2 amino acid transporter as a mediator of glutamine efflux. J. Neurochem. 1999;73(5):2184–94. https://doi.org/10.1046/j.1471-4159.1999.02184.x.
[83] Dolińska M, Zabłocka B, Sonnewald U, Albrecht J. Glutamine uptake and expression of mRNA's of glutamine transporting proteins in mouse cerebellar and cerebral cortical astrocytes and neurons. Neurochem. Int. 2004;44(2):75–81. https://doi.org/10.1016/S0197-0186(03)00123-2.
[84] Jeon GS, Choi DH, Lee HN, Kim DW, Chung CK, Cho SS. Expression of l-Serine Biosynthetic Enzyme 3-Phosphoglycerate Dehydrogenase (Phgdh) and Neutral Amino Acid Transporter ASCT1 Following an Excitotoxic Lesion in the Mouse Hippocampus. Neurochem. Res. 2009;34(5):827–34. https://doi.org/10.1007/s11064-008-9831-5.
[85] Pfrieger FW, Ungerer N. Cholesterol metabolism in neurons and astrocytes. Prog. Lipid Res. 2011;50(4):357–71. https://doi.org/10.1016/j.plipres.2011.06.002.
[86] Abramov AY, Ionov M, Pavlov E, Duchen MR. Membrane cholesterol content plays a key role in the neurotoxicity of β-amyloid: Implications for Alzheimer's disease. Aging Cell 2011;10(4):595–603. https://doi.org/10.1111/j.1474-9726.2011.00685.x.